A Micromirror With Large Static Rotation and Vertical Actuation

Jin-Chern Chiou, Chin-Fu Kou, and Yung-Jiun Lin

***Abstract*—A micromirror with large rotation angle and vertical displacement is proposed and developed. The proposed micromirror is actuated by newly developed prestress comb drive actuators, which exhibit no pull-in, no hysteresis, and large vertical displacement range characteristics. The micromirror was fabricated using commercially available PolyMUMPs. Experimental results indicated that the maximum rotation angle and vertical displacement of the device are 26 and 45 μm, respectively.**

***Index Terms*—Microelectromechanical systems (MEMS), micromirror, microoptoelectromechanical systems (MOEMS), prestress comb drive actuator (PCA).**

I. Introduction

RECENTLY, microelectromechanical systems (MEMS)-based micromirrors have been applied in optical switch and displays [1]–[3]. They are also used in a wide range of applications such as interferometric systems [4], confocal microscopes [5], wavelength-selective switches [6]–[9], variable optical attenuators [10], and biomedical image [11]–[13]. MEMS-based micromirrors have higher operating speed and lower mass than that of traditional fabricated technology, and potential for lower cost through MEMS fabrication process. A successful example of MEMS-based micromirrors is Texas Instrument's digital micromirror device (DMD) [14].

In most applications, electrostatic actuators are preferred because of their low power consumptions. Most of the micromirrors reported to date employ the parallel-plate electrostatic actuator. It is relatively simple in terms of design and fabrication; however, it suffers from the pull-in phenomenon, which limits its useful scan range. To overcome the pull-in phenomenon, vertical comb drive actuators have been developed. The vertical comb drive is considered to be regarded as the most feasible technique for obtaining large angular motion. Here, angular motion plays an important role in optical applications such as digital switching [15], [16] and raster scanning [17], [18]. Recently, a high aspect ratio micromachining process using electroplating, deep reactive ion etch (DRIE), and inductively coupled plasma (ICP) has been demonstrated to be important in further increasing an even larger angular motion [19]. Si dry etching is carried out from the top and bottom surfaces of the silicon-on-insulator (SOI) wafer in constructing a vertical comb. However, these methods are difficult to implement, because they need complex fabrication process, and may easily cause the problems of misalignment and gap-expansion problems [20]–[22].

In this regard, a prestress comb drive actuator (PCA) that is capable of achieving no pull-in, no hysteresis, and large vertical displacement range characteristics is developed to overcome the limitations of the actuation range of the aforementioned electrostatic actuator and achieve out-plane degree of freedom [23]. In this paper, a micromirror device that consists of two PCAs is proposed to achieve large rotation and vertical actuation. The device is fabricated through commercial available PolyMUMPs. This paper is organized as follows. First, we describe the design and analysis of the PCA. Next, we present the design and fabrication of the micromirror. Finally, we report the measurement results including static dc scanning characteristic and frequency response.

Manuscript received October 2, 2006; revised October 19, 2006. This work was supported in part by the Ministry of Economic Affairs, Taiwan, R.O.C., under Contract 91-EC-17-A-07-S1-0011, and in part by the National Science Council, Taiwan, R.O.C., under Contract NSC 94-2218-E-009-031 and Contract NSC 94-2215-E-009-056, and in part by the MOE ATU Program.

The authors are with the Department of Electrical and Control Engineering, National Chiao Tung University, Hsinc, 30010, Taiwan, R.O.C. (e-mail: chiou@mail.nctu.edu.tw; kcf22@seed.net.tw; yjlin@mail.nctu.edu.tw).

Digital Object Identifier 10.1109/JSTQE.2007.892069

II. Actuator Design and Its Working Principle

A. Actuator Design

Surface micromachining provides a flexible mechanical and electrical structure. Here, the working/motion space of various actuators is limited in in-plane actuation or small out-plane motion displacement [17]. Chen *et al.* used the stress-induced bending of a composite cantilever beam to raise a vertical mirror mounted in the free end [24]. A cantilever beam with a length of 1500 μm with a 300-μm vertical displacement is developed [24]. Its driving mechanism is similar to that of a parallel-plate electrostatic actuator that has the drawback of pull-in, which limits its applications. The mechanical stability of the actuator becomes crucial when it is applied to other MEMS devices that require analog tuning. Rosa *et al.* proposed an external electrode concept that contrasts with the conventional concept and frequently employed a parallel-plate electrode scheme for the electrostatic actuation of MEMS devices [25]. The external electrode configuration allows the operation of electrostatic actuators to be controlled over their entire range of motion by preventing electrostatic pull-in instability. It is based on the application of the fringe effect between the moving electrode and the fixed external electrodes. Notably, the shape of the external electrodes seems to be designed arbitrarily. However, the fringe effect between the moving and fixed external electrodes is relatively inefficient. Accordingly, the static characteristic criteria in obtaining the actuating force of the electrostatic actuator are severely limited. Akiyama *et al.* have demonstrated a comb-shape electrostatic actuator for high-speed feedback motion, with which they achieved almost 1-μm stroke under 50–130 applied voltages when the initial height difference, due to the residual stress, was 2 μm [26].

1077-260X/$25.00 © 2007 IEEE

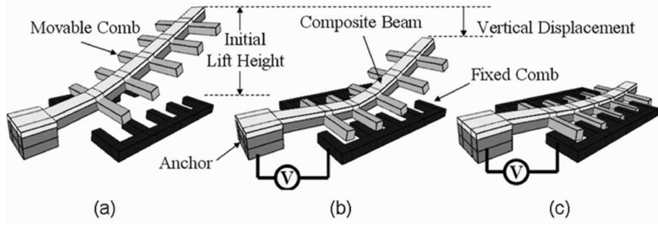

Fig. 1. PCA at different driving states. (a) Initial state. (b) Bias voltage state. (c) Critical bias voltage state.

In this regard, a PCA that could overcome the limitations of the actuation range of the aforementioned electrostatic actuator and achieve an out-plane degree of freedom was developed [23]. Fig. 1 schematically depicts a PCA with different driven states. The PCA consists of an anchor, a composite beam, and a set of comb fingers. These comb fingers, designed along the composite beam and substrate, acted as the movable and fixed comb fingers. Fig. 1(a) shows one end of the composite beam, which is clamped to the anchor while the other end is elevated due to the residual stress between the two deposited materials. Notably, the initial lift height of the PCA can be further enhanced by increasing the residual stress of the composite beam using a postheat treatment process [24]. When a voltage V is applied between the movable and fixed comb, the movable composite beam could be pulled downward to the substrate by the electrostatic force induced by the fringe effect, as shown in Fig. 1(b). The taper-like distances between each movable and fixed comb are obtained from the free end to the fixed end based on the curved-up shape of the composite beam. In the actuating mechanisms, the movable comb fingers that are closed to the anchor provide the main actuation force. As the actuation progresses, the retral movable comb fingers will be pulled down accordingly. As the driving voltage is increased, the vertical displacement of the free end of the PCA is increased. Notably, the electrostatic force is constrained when the movable comb finger is closed to the fixed comb finger, independent of the input driving voltage. Therefore, the vertical electrostatic force approaches zero as the movable comb finger reaches its equilibrium position. Fig. 1(c) demonstrates that, when a critical bias voltage is applied between the movable and fixed comb, the PCA will land itself to the substrate.

B. Modeling and Simulation

The PCA cantilever composite beam consists of two materials A and B that possess tensile and compress residual stress, respectively, as shown in Fig. 2(a). With the released and heat treatment processes, the composite beam is assumed curving up with lift height H_L at the free end due to the induced stresses. In the present derivations, the symbols $a_n, P_n, H_{\mathrm{Fn}}$, and L represent the distance related to the anchor, electrostatic force induced by the comb finger $1-n$ in kth and ($k-1$)th state, lift height of the nth movable comb finger, and length of composite beam, respectively. Here, one-movable and two-fixed comb fingers were defined as a single pair of comb fingers for the purpose of simulating and extracting capacitance function during electrostatic force calculation. A cross-section view of the PCA is shown in Fig. 2(b), where L_C is the engaged length between the movable and fixed comb fingers.

1) Decomposition of Multiple Loads: In the mechanics of material analysis, the deflection of a straight beam with constant multiple loads can be calculated as follows [26]:

$$\begin{cases} z_{xn} = \frac{P_n x^2}{6E_c I_c}(3a_n - x) \\ z'_{xn} = \frac{P_n x}{2E_c I_c}(2a_n - x) \end{cases}, \quad \text{for } 0 \le x \le a \tag{1}$$

$$\begin{cases} z_{xn} = \frac{P_n a_n^2}{6E_c I_c}(3x - a_n) \\ z'_{xn} = \frac{P_n a_n^2}{2E_c I_c} \end{cases}, \quad \text{for } a_n \le x \le L \tag{2}$$

where x is the position of the beam, z_{xn} is the shape of small deflection of strength beam of position x from the nth load, z'_{xn} is the slope of shape of position x from the nth load, a_n is the position of the nth load, P_n is the electrostatic force induced by the comb finger $1-n$ in kth and ($k-1$)th state, E_c is the Young's module of equivalent single material beam, and I_c is the moment of inertia of equivalent single material beam. The following section discusses the equivalent material parameters and electrostatic force.

2) Moment of Inertia of Composite Beam: In order to accurately calculate the moment of inertia of the designed beam, the composite beam can be recast into a T-shaped single beam, as shown in Fig. 3.

The material A with width b was replaced by material B with width αb, where b is the width of the composite beam, α is the proportional constant between the Young's module of materials A and B, h_1 is the distance between the top side of material A and neutral axis of T-shaped beam, and h_2 is the distance between the bottom side of material B and neutral axis of T-shaped beam. The moment of inertia of T-shaped beam can be expressed as [27]

$$I_c = \frac{1}{12}bt_A^3 + bt_A\left(h_1 - \frac{t_A}{2}\right)^2 + \frac{1}{12}(\alpha b)t_B^3 + \ldots + \alpha bt_B\left(h_2 - \frac{t_B}{2}\right)^2 \tag{3}$$

where $E_c = E_B$, $\alpha = E_B/E_A, h_1 = (t_A A_A + t_B A_B)/(A_A + A_B), h_2 = t_A + t_B - h_1$, and A_A and A_B are the cross-section areas of materials A and B, respectively.

3) Extraction of Electrostatic Force: In general, the electrostatic force of a comb drive can be expressed as [28]

$$F_E = \frac{1}{2}NL_C\frac{dC}{dz}V^2 \tag{4}$$

where N is the number of comb fingers, L_C is the engaged length of comb fingers, *dC/dz* is the gradient of capacitance of comb fingers in z-motion direction, and V is the applied dc bias voltage. In a static state case, N, L_C, and V^2 are constant, and the *dC/dz* term, the electrostatic force index, is a function of z [29]. In order to extract the function accurately, an electromagnetic simulation software AnSoft/Maxwell 2D was employed to calculate the comb finger capacitance at different z-positions.

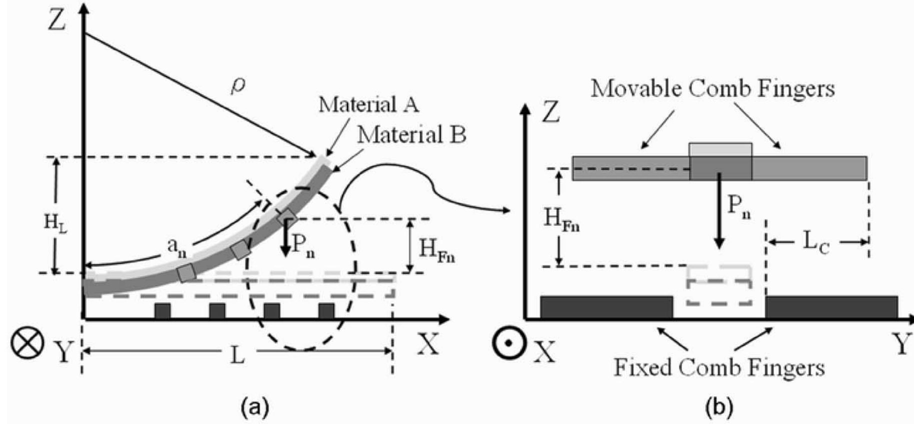

Fig. 2. Schematic of the PCA. (a) *XZ* plane cross-section view. The circle indicates a single pair of comb finger. (b) *YZ* plane cross-section view.

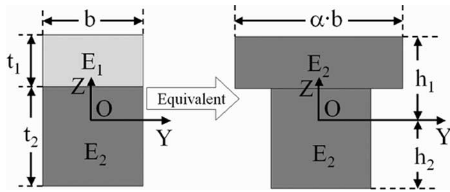

Fig. 3. Equivalent beam model of the composite beam.

By using Matlab simulation software, a sixth-order curve fitting was used to extract the capacitance function $C(z)$ and the electrostatic force index was obtained by the derivative of the capacitance function. The electrostatic force can be rewritten as

$$F_{En}(z, V) = \frac{1}{2} N L_C (C_0 z^6 + C_1 z^5 + C_2 z^4 + C_3 z^3 + C_4 z^2 + C_5 z^1 + C_6) V^2 \quad (5)$$

where $F_{En}(z, V)$ is the unit electrostatic function of the nth single pair of comb drive in the PCA. Since each movable comb finger has different position, the electrostatic force contributed from each comb finger is experiencing taper-like behavior from fixed end to free end. Consequently, P_n denotes the difference of electrostatic force induced by the comb finger $1-n$ in kth and $(k-1)$th state that can be expressed as

$$P_n = F_{En}(z, V_k) - F_{En}(z, V_{k-1}). \quad (6)$$

Fig. 4 shows the simulation result of a single pair of comb drive. The simulation data are calculated by AnSoft/Maxwell 2D, and fit very well by the sixth-order polynomial $C(z)$.

Table I presents the static analysis of the PCA with related simulation parameters. The shape of the PCA is determined by assuming the initial curvature of the composite beam. At a given curvature, a PCA is obtained with an initial lift height of 110 μm. The material properties in the present simulation were based on the reference from PolyMUMPs process [30].

Fig. 5 reveals the primary simulation results of the PCA obtained by applying various voltages. Notably, the lift height is represented by the tip height at the free end of the PCA. Fig. 5 clearly indicates that the typical pull-in behavior of parallel-plate electrostatic actuators was not observed in the present design. Notably, in the early actuation stage, the electrostatic force obtained from the elevated comb fingers overwhelms the spring force exerted in the composite beam, creating a steep gradient at certain applied voltages (80–120 V in the design

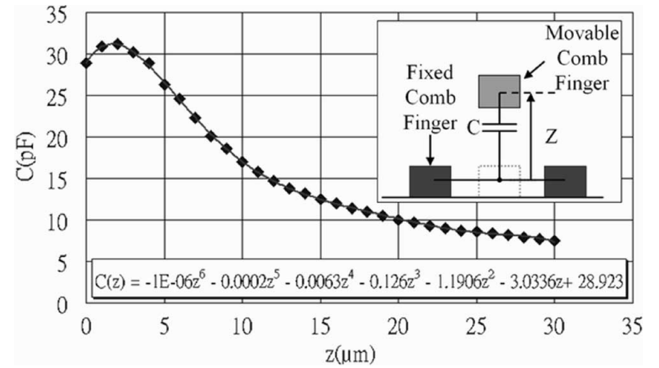

Fig. 4. Capacitance versus displacement simulation of single-pair comb drive.

TABLE I
PARAMETERS OF PRIMARY SIMULATION

Symbol	Value
L	540μm
L_c	40μm
n	34
a_1 ~a_n	40~500μm
ρ	1450μm
b	40μm
E_A	78 Mpa
E_B	160 Mpa
V	0~200V
t_A	0.5μm
t_B	1.5μm
C_0	-1E-18
C_1	- 2E-16
C_2	- 6E-15
C_3	- 1E-13
C_4	- 1E-12
C_5	- 3E-12
C_6	3E-11

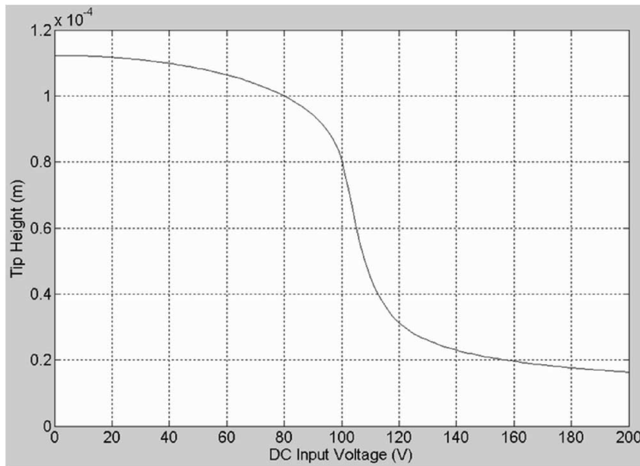

Fig. 5. Steady-state simulation results of the PCA.

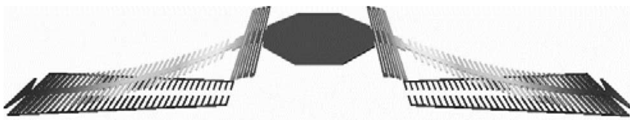

Fig. 6. Schematic of the micromirror device.

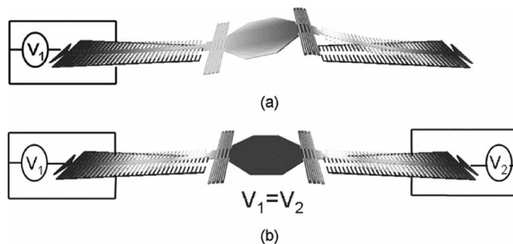

Fig. 7. FEM simulation results. (a) Rotation mode. (b) Piston (vertical actuation) mode.

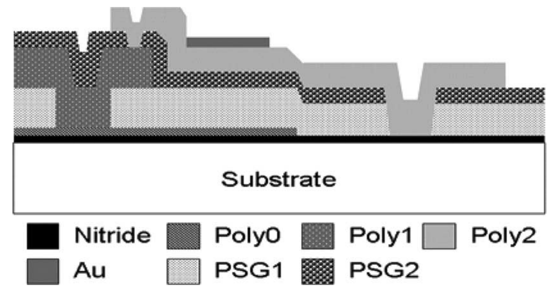

Fig. 8. Cross-sectional view of PolyMUMPs process.

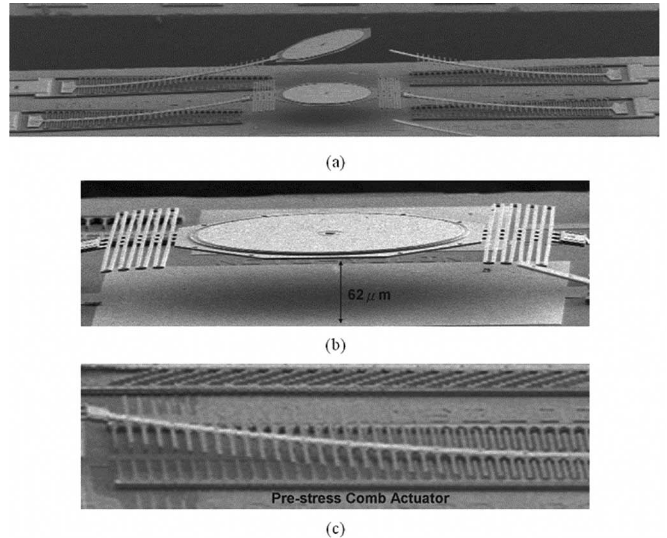

Fig. 9. SEM images of the fabricated micromirror device. (a) Micromirror device. (b) Mirror and springs. (c) PCA.

herein). However, when most of the movable comb fingers made the contact with the substrate at applied voltages higher than 120 V, the gradient variation becomes insignificant due to the decreased of effective comb fingers, as depicted in Fig. 1.

III. Micromirror Device Design and Fabrication

Fig. 6 depicts the micromirror device investigated in this paper schematically. The device contains a micormirror, springs, and a pair of PCAs. The two PCAs are connected to the mirror by the springs in confronting positions. Upon releasing the PCAs, the micromirror is elevated from the substrate. By actuating the PCAs, the micromirror could achieve rotation and vertical actuation. Fig. 7 shows the finite element method (FEM) simulation results of the operation modes. As illustrated in Fig. 7(a), the micromirror could achieve rotation motion by applying driving voltage to one of the PCAs. By applying the same driving voltage to the pair of the PCAs, the micromirror could realize pure vertical motion, as illustrated in Fig. 7(b).

The proposed micromirror device was fabricated using the commercial available PolyMUMPs process [30]. This process consists of a nitride isolation layer, three polysilicon structural layers (Poly0–2), two phosphosilicon glass sacrificial layers (PSG1 and PSG2), and a gold metal layer (Au) for optical reflection and electronic connection. After dicing process, hydroflouric (HF) acid is used to release the MEMS structures. Fig. 8 depicts the cross-section view of the PolyMUMPs process. In this paper, the postheat treatment is needed for the released device. It could increase the residual stress of composite beam. To treat the device, it needs to be heated at 170 °C for 10 s to complete the postheat treatment. Fig. 9 shows the scanning electron microscopy (SEM) images of the fabricated device after release process and postheat process. The mirror and spring are shown in Fig. 9(b), and the PCA is shown in Fig. 9(c). Both PCAs consist of a 540 μm $\times$ 40 μm composite beam that is fixed to an anchor structure with 34 movable comb fingers orthogonally mounted on the composite beam, and 35 fixed comb fingers are mounted on the surface of the nitride. Here, the engaged length of the comb finger is designed to be 40 μm. The composite beam was accomplished by depositing a 0.5-μm-thick Au film on the surface of the 1.5-μm-thick polysilicon (Poly2). Based on the tensile and compress residual stress of Au and Poly2 layer, the composite beam is exhibited a curved-up out-of-plane behavior. To prevent unneeded residual stress on the movable comb fingers, Au film was not deposited on top of

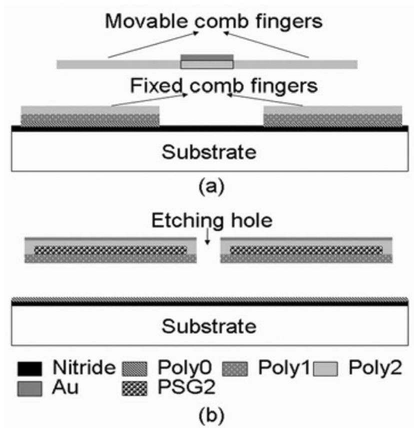

Fig. 10. Cross-sectional view of the micromirror device. (a) PCA. (b) Mirror.

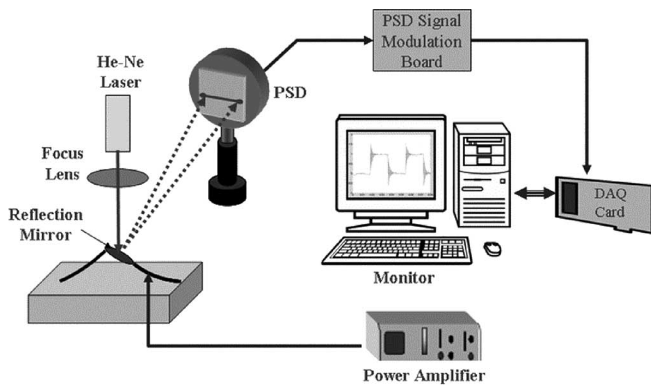

Fig. 11. Schematic of the measurement system.

the Poly2 layer of the movable comb fingers. The fixed comb fingers were manufacture by stacking up Poly0, Poly1, and Poly2. The diameter of the mirror is 200 μm. A metal layer (Au) was deposited on the mirror to obtain high reflect efficiency. The cross-section view of the PCA is illustrated in Fig. 10(a). In order to minimize the curvature of the mirror surface, the multilayer structure design had been used. The PSG2 (0.75 μm) was trapped between two polysilicon layers (Poly1 and Poly2). Fig. 10(b) shows the cross-section view of the mirror. After release process and postheat treatment, the micromirror is elevated 62 μm by the PCAs.

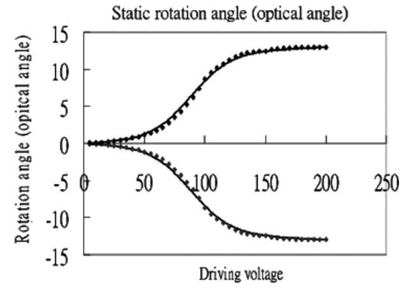

Fig. 12. Static rotation angle of the fabricated micromirror versus driving voltage.

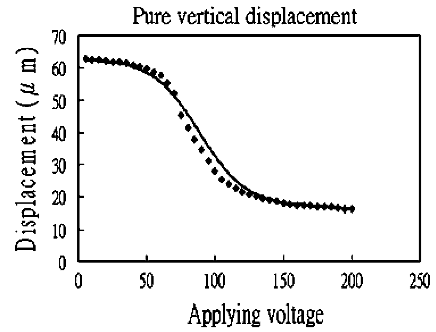

Fig. 13. Pure vertical displacement of the fabricated micromirror versus driving voltage.

TABLE II
MODE SHAPE OF THE MICROMIRROR

Mode	Frequency (Hz)	Motion	Solid mode shape
First mode	2198.7	Pitch	
Second mode	6520.4	Pitch	
Third mode	15780	Roll	
Fourth mode	30547	Pitch	
Fifth mode	35553	Yaw	

IV. EXPERIMENTAL RESULTS

In order to test the static rotation characteristic of the micromirror device, a measurement system is configured. Fig. 11 is the schematic of the measurement system. A laser beam is generated by He–Ne laser and focused on the reflection mirror by the focus lens. A position-sensitive detector (PSD) is set up to detect the light spot of reflection beam. The PSD array has a current output of the incident beam on the array, and the PSD signal modulate board processes the current signal to the voltage signal. Fig. 12 shows the static rotation characteristics. The dots are measured data while the solid lines are obtained by the theoretical simulation discussed previously. The mirror could be rotated from -6.5° to $+6.5^\circ$ in mechanical angle, resulting in a maximum optical scanning angle of 26°. To measure the vertical displacement of the micromirror, an optical interferometric profiler (WYKO) was used. Fig. 13 shows the experimental and simulated results. The vertical displacement decreases from 62 to 17 μm when driving voltage increases from 0 to 200 V; thus, a maximum vertical displacement of 45 μm is observed.

From the experimental and simulation results, we have observed that the tip of the free end will not make contact with the substrate due to the fact that we have designed a 40-μm length of the beam region without either movable or fixed comb fingers.

To fully understand the resonant characteristics of the PCA, a FEM simulator, IntelliSuite, was used to calculate the resonant frequencies and the corresponding mode shapes. Table II

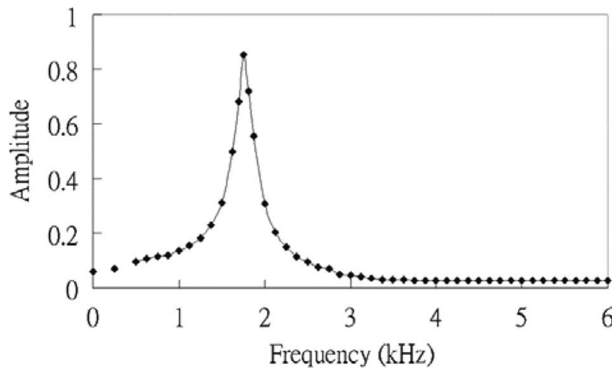

Fig. 14. Frequency response of the fabricated micromirror.

presents the mode shape simulation results of the proposed micromirror. If the third and fifth modes, corresponding to the roll and yaw motion of the device, are excited, the device might be damaged. In addition, a MEMS motion analysis (MMA) was used to measure the frequency response of the device. Fig. 14 shows the measurement result of the frequency response with 20-V driving voltage. The resonant frequency is obtained from the peak of the frequency response curve, and the resonant frequency is 1.8 kHz. The differences between the measured and the simulated values are mainly due to fabricated variation and air damping.

V. Conclusion

In this paper, a micromirror with large rotation angle and vertical displacement was investigated. The micromirror is actuated by two PCAs, and the device was fabricated through commercial available PolyMUMPs without additional fabrication process. Experimental results indicated that the maximum optical scanning angle and pure vertical displacement of the micromirror are 26 and 45 μm, respectively. Potential applications of this dual mode include optical scanners, optical switches, medical imaging, optical phased arrays, and displays.

References

[1] R. Ryf *et al.*, "1296-port MEMS transparent optical cross connect with 2.07 petabit/s switch capacity," in *Tech. Dig. Opt. Fiber Commun. Conf.*, Anaheim, CA, Mar. 2001, Paper PD-28.

[2] P. M. Hagelin, U. Krishnamoorthy, J. P. Heritage, and O. Solgaard, "Scalable optical cross-connect switch using micromachined mirrors," *IEEE Photon. Technol. Lett.*, vol. 12, no. 7, pp. 882–884, Jul. 2000.

[3] M. O. Freeman, "Miniature high-fidelity displays using a biaxial MEMS scanning mirror," *Proc. SPIE*, vol. 4985, pp. 56–62, 2003.

[4] F. A. Chollet, G. M. Hegde, A. K. Asundi, and A. A. Liu, "Simple extra short external-cavity laser self-mixing interferometer for acceleration sensing," *Proc. SPIE*, vol. 4596, pp. 272–279, 2001.

[5] K. Murakami, A. Murata, T. Suga, H. Kitagawa, Y. Kamiya, M. Kubo, K. Matsumoto, H. Miyajima, and M. Katashiro, "A miniature confocal optical microscope with MEMS gimbal scanner," in *Proc. Transducers*, Boston, MA, 2003, pp. 587–590.

[6] D. M. Marom *et al.*, "Wavelength-selective 1 × 4 switch for 128 WDM channels at 50 GHz spacing," in *Tech. Dig. Opt. Fiber Conf.*, Anaheim, CA, Mar. 2002, Paper FB7.

[7] D. Hah, S. Huang, H. Nguyen, H. Chang, H. Toshiyoshi, and M. C. Wu, "A low voltage, large scan angle MEMS micromirror array with hidden vertical comb drive actuators for WDM routers," in *Tech. Dig. Opt. Fiber Conf.*, Anaheim, CA, Mar. 2002, pp. 92–93.

[8] D. Hah, S. Huang, H. Nguyen, H. Chang, J.-C. Tsai, H. Toshiyoshi, and M. C. Wu, "Low voltage MEMS analog micromirror arrays with hidden vertical comb drive actuators," in *Tech. Dig. Solid-State Sens., Actuator, Microsyst. Workshop*, Hilton Head Island, SC, Jun. 2002, pp. 11–14.

[9] T. Ducellier *et al.*, "The MWS 1 × 4: A high performance wavelength switching building block," in *Tech. Dig. 28th Eur. Conf. Opt. Commun.*, Copenhagen, Denmark, Sep. 8–12, 2002.

[10] C. Marxer, P. Griss, and N. F. de Rooij, "A multichannel variable optical attenuator for power management in fiber optic networks," in *Proc. 10th Int. Conf. Sens. Actuators*, Sendai, Japan, Jun. 1999, pp. 798–799.

[11] W. Piyawattanametha, L. Fan, S. Hsu, M. Fujino, M. C. Wu, P. R. Herz, A. D. Aguirre, Y. Chen, and J. G. Fujimoto, "Two-dimensional endoscopic MEMS scanner for high resolution optical coherence tomography," in *Proc. CLEO*, San Francisco, CA, 2004, Paper CWS2.

[12] U. Hofmann, S. Muehlmann, M. Witt, K. Dorschel, R. Schutz, and B. Wagner, "Electrostatically driven micromirrors for a miniaturized confocal laser scanning microscope," *Proc. SPIE*, vol. 3878, pp. 29–38, 1999.

[13] Y. Pan, H. Xie, and G. K. Fedder, "Endoscopic optical coherence tomography based on a CMOS-MEMS micromirror," *Opt. Lett.*, vol. 26, pp. 1966–1968, 2001.

[14] L. J. Hornbeck, "Current status of the digital micromirror device (DMD) for projection television applications," in *IEDM Tech. Dig.*, 1993, pp. 381–384.

[15] M. Mita, D. Miyauchi, H. Toshiyoshi, and H. Fujita, "An out-of-plane polysilicon actuator with a smooth vertical mirror for optical fiber switch application," in *Proc. IEEE/LEOS Summer Topical Meetings* Jul. 20–24, 1998, pp. II/33–II/34.

[16] W. C. Chen, C. Y. Wu, and C. K. Lee, "Bi-directional movable latching structure using electrothermal V-beam actuators for optical switch application," in *Proc. IEEE/LEOS Opt. MEMS,* Aug. 18–21, 2003, pp. 149–150.

[17] W. Piyawattanametha, P. R. Patterson, H. Dooyoung, H. Toshiyoshi, and M. C. Wu, "A 2D scanner by surface and bulk micromachined vertical comb actuators,," in *Proc. IEEE/LEOS Opt. MEMS,* Aug. 18–21, 2003, pp. 93–94.

[18] R. A. Conant, J. T. Nee, K. Y. Lau, and R. S. Muller, "Dynamic deformation of scanning mirrors," in *Proc. Opt. MEMS*, 2000, pp. 49–50.

[19] C. C. Chu, J. M. Tsai, J. Hsieh, and W. Fang, "A novel electrostatic vertical comb actuator fabricated on [111] silicon wafer," in *Proc. IEEE MEMS*, 2003, pp. 56–59.

[20] J.-H. Lee, Y.-C. Ko, and H.-M. Jeong, "SOI-based fabrication processes of the scanning mirror having vertical fingers," *Sens. Actuators A*, vol. 102, pp. 11–18, 2002.

[21] S. Kwon, V. Milanovic, and L. P. Lee, "Vertical combdrive based 2-D gimbaled micromirrors with large static rotation backside island isolation," *IEEE J. Sel. Topics Quantum Electron.*, vol. 10, no. 3, pp. 498–504, May/Jun. 2004.

[22] M. Sasaki, D. Briand, W. Noell, and N. D. Rooij, "Vertical comb drive actuator constructed by buckled bridges in SOI-MEMS,," in *Proc. IEEE/LEOS Opt. MEMS,* Aug. 18–21, 2003, pp. 89–90.

[23] J. C. Chiou and Y. J. Lin, "A novel large displacement electrostatic actuator: Pre-stress comb drive actuator," *J. Micromech. Microeng.*, vol. 15, pp. 1641–1648, 2005.

[24] R. T. Chen, H. Nguyen, and M. C. Wu, "A low voltage micromachined optical switch by stress-induced bending," in *Proc. IEEE MEMS',* Jan. 17–21, 1999, pp. 424–428.

[25] M. A. Rosa, D. D. Bruyker, A. R. Volkel, E. Peeters, and J. Dunec, "A novel external electrode configuration for the electrostatic actuation of MEMS based devices," *J. Micromech. Microeng.*, vol. 14, pp. 446–451, 2004.

[26] T. Akiyama, U. Staufer, and N. F. Rooij, "Atomic force microscopy using an integrated comb-shape electrostatic actuator for high-speed feedback motion," *Appl. Phys. Lett.*, vol. 76, no. 21, pp. 3139–3141, May 2000.

[27] J. M. Gere and S. P. Timoshenko, *Mechanics of Materials*, 3rd ed. Boston, MA: PWS-Kent, 1990, pp. 301–308, 465, 772.

[28] H. Xie and G. K. Fedder, "Vertical comb-finger capacitive actuation and sensing for CMOS-MEMS," *Sens. Actuators*, vol. A 95, pp. 212–221, 2002.

[29] J. C. Chiou and Y. J. Lin, "A new modeling method of vertical electrostatic comb drive," *J. Comput. Eng. Sci.*, vol. 4, pp. 641–644, 2003.

[30] D. Koester *et al.*, "PolyMUMPs Design Handbook," rev. 10, MEMSCAP, 2003.

Jin-Chern Chiou received the M.S. and Ph.D. degrees in aerospace engineering science from the University of Colorado at Boulder, Boulder, in 1986 and 1990, respectively.

During 1991–1992, he was a Research Associate at the Center for Space Structure and Control, University of Colorado at Boulder. Since 1992, he has been with the Department of Electrical and Control Engineering, National Chiao Tung University (NCTU), Hsinchu, Taiwan, R.O.C. His current research interests include MEMS, fuzzy-logic modeling and control of chemical vapor deposition process, servo control of compact disc–read only memory (CD-ROM) and DVD, and modeling and control of multibody dynamic systems (MBD). He is the coauthor of advanced reference books on CD-ROM system technology and mechanics and control of large flexible structures. He is the holder of two U.S. and three Taiwanese patents.

Dr. Chiou is the recipient of several awards from the Acer Foundation, NCTU, and the National Science Council, Taiwan, R.O.C., for his outstanding research on CD-ROM and MEMS.

Chin-Fu Kuo received the B.S. degree in autocontrol engineering from Feng Chia University, Taichung, Taiwan, R.O.C., in 1999, and the M.S. degree in electrical engineering from I-Shou University, Kaohsiung, Taiwan, in 2001. He is currently working toward the Ph.D. degree in electrical and control engineering at National Chiao Tung University, Hsinchu, Taiwan.

His current research interests include microelectromechanical systems (MEMS) design and applications.

Yung-Jiun Lin received the B.S. and M.S. degrees in autocontrol engineering from Feng Chia University, Taiwan, R.O.C., in 1997 and 1999, respectively, and the Ph.D. degree in electrical and control engineering from the National Chiao Tung University, Taiwan, R.O.C., in 2005.

During 2006, he was a Postdoctoral fellow at the Micro-System and Control Laboratory and Brain Research Center, National Chiao Tung University. Since December 2006, he has been a Research Assistant Professor at the National Chiao Tung University. His current research interests include MEMS/CMOS design and application on optical system, smart sensor, and biomedicine.